Carbonization-driven motion of Si islands on epitaxial graphene

Hiroki Hibino [1,2] and Hiroyuki Kageshima [3]
[1]School of Engineering, Kwansei Gakuin University, Sanda, Hyogo 669-1330, Japan
[2]NTT Basic Research Laboratories, NTT Corporation, Atsugi, Kanagawa 243-0198, Japan
[3]Graduate School of Natural Science and Technology, Shimane University, Matsue, Shimane 690-8504, Japan

(Received 3 February 2023; accepted 24 April 2023; published 15 May 2023)

We investigate structural changes in Si islands deposited at room temperature on epitaxial few-layer graphene on SiC(0001) during subsequent annealing. Annealing causes the Si islands move on epitaxial graphene thicker than monolayer with monolayer-deep trenches left behind. In contrast, Si islands do not form trenches on monolayer graphene, but the Si atoms are intercalated to form quasifreestanding bilayer graphene. The islands which terminated their motion are made of SiC. During annealing, Si islands are carbonized into SiC islands by incorporating carbon atoms from graphene, resulting in the etching of graphene. The carbonization reaction of Si is a driving force of the motion of the Si islands.

DOI: 10.1103/PhysRevMaterials.7.054003

I. INTRODUCTION

Graphene, a two-dimensional crystal of carbon atoms arranged in a honeycomb lattice, has been attracting intense attention due to its novelty in science and expectations to a wide range of applications. Single-crystal graphene substrate is a requisite of device applications of graphene. As for scalable graphene production methods, chemical vapor deposition (CVD) on catalytic metal substrates and thermal decomposition of SiC have been investigated actively. The latter method has an advantage of fabricating graphene devices on wide-band-gap SiC substrates without any transfer processes inevitable to CVD-grown graphene. Epitaxial graphene on SiC wafers could serve as a base for large-scale integration of graphene devices [1,2].

In the thermal decomposition of SiC, Si atoms are preferentially sublimated from the substrates, and the remained carbon atoms naturally form graphene. The first graphitic layer loses graphenelike electronic structures due to chemical bonding with the SiC substrate and is usually called the buffer (or zeroth) layer. A new buffer layer is formed at the interface between the existing buffer layer and the SiC substrate, resulting in transformation of the existing one into epitaxial graphene. Owing to many efforts to control the uniformity of epitaxial graphene, homogeneous monolayer (ML) graphene can now be grown routinely on SiC(0001) substrates in an Ar ambient [3]. However, there is still a basic question about the growth mechanism. Epitaxial graphene growth requires diffusion of Si atoms through the graphene layers. In fact, it is known that the growth rate of epitaxial graphene slows down as it thickens [4]. However, this still seems to contradict with the reported complete impermeability of defect-free graphene to all gases and liquids including He [5]. Only proton is known to be transported through graphene with a low activation energy less than 1.0 eV [6,7]. Hydrogen gas permeation through graphene is also attributed to a two-stage process, which involves flipping of dissociatively chemisorbed hydrogen atoms to the other side of graphene as a rate-limiting process [8]. Understanding of the diffusion path of Si atoms through graphene could contribute to precise control of the number of layers beyond the ML.

Furthermore, it has been demonstrated that intercalation of foreign atoms at the buffer layer/SiC interface is a useful method to modify the electronic transport properties of epitaxial graphene. Various elements, such as H [9], Li [10], O [11], Au [12], F [13], Ge [14], and Si [15–17], have been intercalated. However, the first-principles calculations showed that, even for hydrogen, the diffusion barrier of chemisorbed atoms through the buffer layer is too high to be overcome at temperatures experimentally used for intercalation, and suggested that the hydrogen diffusion occurs through hollow defects in graphene layers [18]. Experimentally, it was found that hydrogen intercalation is not initiated from the curved graphene at the substrate steps, but throughout the buffer layer on the terraces, suggesting that intrinsic defects in the buffer layer may have helped the hydrogen penetration [19]. On the other hand, Li intercalation was found to deteriorate the quality of graphene, which might suggest that the diffusion of Li atoms through graphene is accompanied by the defect formation [10]. Si intercalation was also found to be possible through the existing defect areas or domain boundaries of the graphene layer [15]. It seems certain that the defects in graphene play essential roles in the intercalation, but the detailed process in the atom diffusion through graphene has not been fully clarified yet.

In this paper, towards the understanding of the diffusion path of Si atoms through graphene, we investigate how Si atoms move on and/or through epitaxial graphene. Si deposition at room temperature forms Si islands on epitaxial graphene. Structural changes of the Si-deposited graphene during annealing are investigated *in situ* using low-energy electron microscopy (LEEM). Annealing induces the motion of Si islands on epitaxial graphene thicker than or equal to bilayer (BL), and the motion is accompanied by ML-deep trenches left behind. During annealing, Si islands are carbonized into SiC islands by incorporating carbon atoms from

 ©2023 American Physical Society

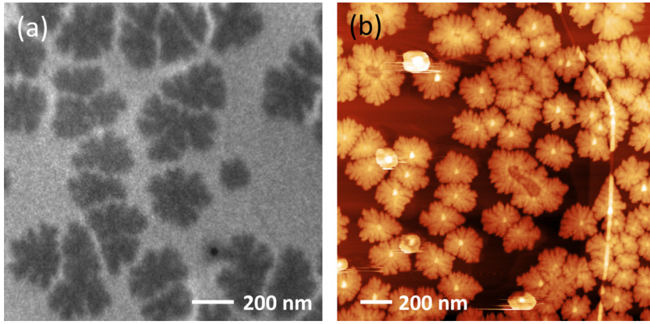

FIG. 1. (a) LEEM and (b) AFM images of epitaxial graphene after deposition of Si nearly equal to the atomic density of silicene at room temperature. The electron-beam energy of (a) was 12.0 eV.

graphene, resulting in the trenches in graphene. On the other hand, Si intercalation rather than trench formation takes place in the ML area. Thinner graphene is more permeable against Si atoms.

II. EXPERIMENTAL

Epitaxial few-layer graphene used for *in situ* LEEM observations of Si island motion was grown on 4H-SiC(0001) by the thermal decomposition at about 1300 °C in a LEEM instrument (ELMITEC LEEM III). The samples were annealed by electron-beam bombardment from the backside, and the sample temperatures were estimated using a WRe thermocouple inside the sample holder. The number of graphene layers was determined from the low-energy electron reflectivity (LEER) spectra [20]. Si was deposited from a directly heated Si piece in the LEEM instrument, and the amount of deposited Si was roughly controlled by the electric current passing through the Si piece and the deposition time. The typical deposited amount of Si was 0.5–1 times of the atomic density of silicene ($1.54 \times 10^{15}\ \mathrm{cm}^{-2}$). The sample surface morphologies were measured *ex situ* using atomic force microscopy (AFM) instruments (Veeco Nanoscope III and Bruker Innova) in the tapping mode. Cross-sectional transmission electron microscopy (TEM) images were also obtained *ex situ* to investigate the atomic structures of the Si-deposited epitaxial graphene after annealing.

III. RESULTS AND DISCUSSION

Figures 1(a) and 1(b) show the LEEM and AFM images of epitaxial graphene after deposition of Si nearly equal to the atomic density of silicene at room temperature. This epitaxial graphene was grown at 1750 °C in Ar (600 Torr) using an infrared furnace. The sample was transferred to the LEEM instrument through air and was annealed before the Si deposition to remove the air-induced adsorbates. The imaged region is mostly covered with ML graphene. The deposited Si islands have a dendritic shape. They prefer to nucleate at the buffer layers [21] and have a weak tendency to nucleate at the substrate steps and the boundaries between the areas with different graphene thicknesses. These dendritic islands are well resembled with the reported Si islands deposited on epitaxial graphene [22]. They exhibit no low-energy electron diffraction spots, indicating that they are in an amorphous phase.

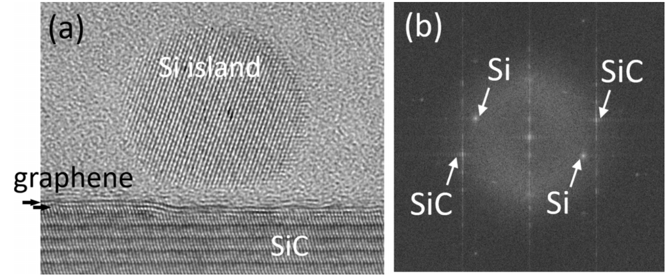

FIG. 2. (a) Cross-sectional TEM image of a Si island after annealing at 900 °C. (b) Fast Fourier transform (FFT) pattern of (a).

Annealing typically above 400 °C caused the island shape to change from dendritic to compact. Figure 2(a) shows a cross-sectional TEM image of a compact three-dimensional island after annealing at 900 °C. A clear lattice image seen in the compact island indicates that the shape transformation of the Si islands is the result of crystallization. The gap between the crystalline Si island and epitaxial graphene is likely to be Si oxide formed after removal from ultrahigh vacuum. The FFT pattern of the TEM image in Fig. 2(b) includes two sets of patterns from the Si island and 4H-SiC substrate. The island looks like a sphere, indicating a weak interaction between the Si island and graphene. It should be also noted that the Si island in Fig. 2(a) is single crystalline and aligned to the substrate lattice, but this is not always the case for all the islands.

Figures 3(a) and 3(b) show AFM height and phase images of Si-deposited epitaxial graphene after annealing at 970 °C. The phase images map the variation in the phase of the

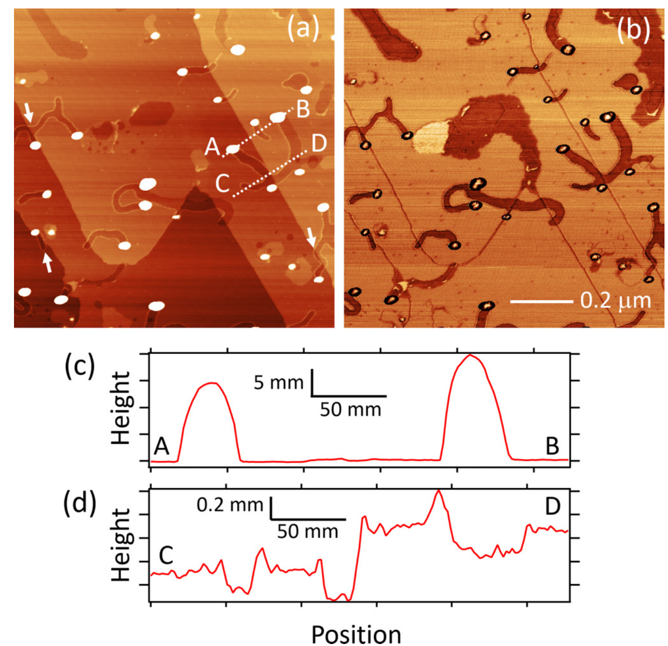

FIG. 3. AFM (a) height and (b) phase images of Si-deposited epitaxial graphene after annealing at 970 °C. (c) and (d) Cross sections between *A* and *B* and between *C* and *D* in (a).

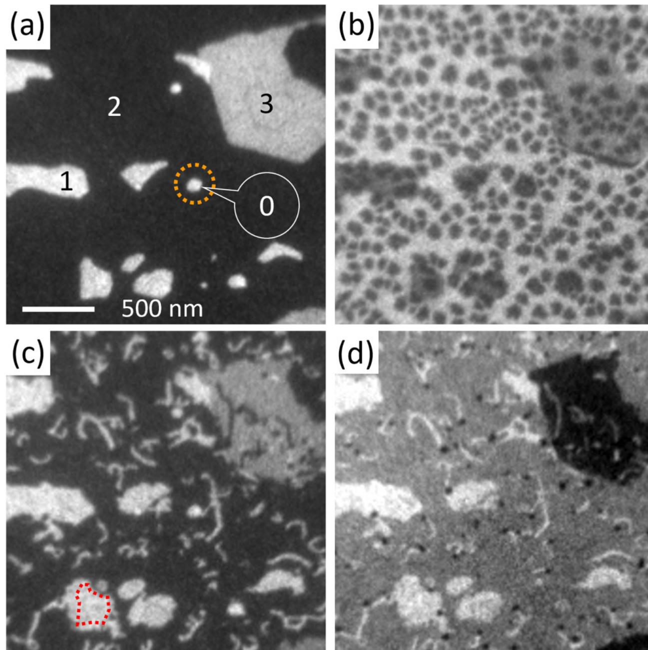

FIG. 4. (a) LEEM image of epitaxial graphene before Si deposition. Numbers in the image indicate the number of epitaxial graphene layers. (b) LEEM image after Si deposition. (c) and (d) LEEM images after annealing at 1130 °C. The red dotted lines in (c) indicate the positions of a representative ML area seen in (a). The electron-beam energies were (a) 4.0, (b) 3.0, (c) 3.8, and (d) 4.8 eV.

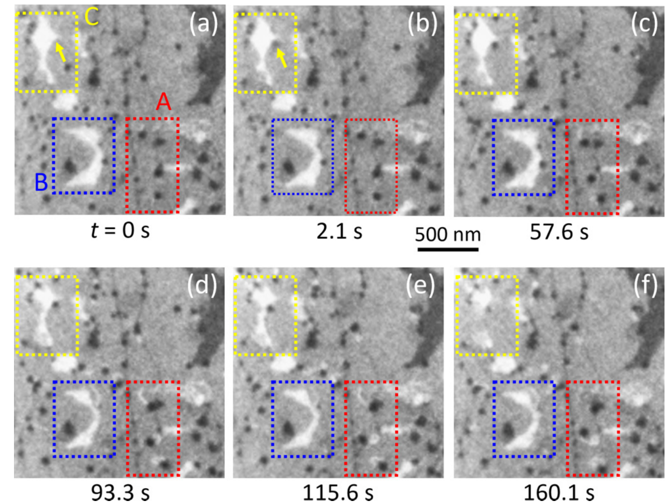

FIG. 5. LEEM images of the Si-deposited epitaxial graphene during annealing at 890−900 °C. The measured time of each image is indicated. The electron-beam energy was 6.7 eV.

oscillating probe tip and can be used to differentiate areas with different materials properties. There are round islands with the height of 5–20 nm as represented by the cross section in Fig. 3(c). We also observe that the islands are linked to trenches, whose depth is approximately 0.2–0.3 nm from Fig. 3(d). The LEEM observations before Si deposition show that this sample is mostly covered with BL graphene. It is also known that few-layer epitaxial graphene provides clear contrasts in the AFM phase images depending on the number of graphene layers [23]. The depth and phase contrast of the trenches suggest that there is ML graphene in the trenches, meaning that ML-deep trenches are formed in BL graphene.

The ML-deep trench formation is also confirmed by LEEM. Figure 4(a) shows a LEEM image of epitaxial graphene before Si deposition. The electron-beam energy was 4.0 eV. As indicated by numbers in the image, the epitaxial graphene mostly consists of BL with some ML and trilayer (TL) areas. Small inclusions of the buffer (zeroth) layer are also observed. In a LEEM image after Si deposition [Fig. 4(b)], dendritic islands are seen. Figures 4(c) and 4(d) show LEEM images after annealing at 1130 °C. Their electron-beam energies were 3.8 and 4.8 eV, respectively. We find many thin linear structures in these images, and there are always black dots (compact islands) at one end of them. The linear structures in the BL and TL areas have image intensities similar to the ML and BL areas, respectively. This means that the linear structures are thinner by ML than the surrounding areas. These LEEM results are consistent with the AFM results that the ML-deep trenches are formed on Si-deposited epitaxial graphene during annealing. Here, we note that no linear structures are found in the ML areas by LEEM. The trench formation is limited to graphene thicker than ML, which will be addressed in detail later.

We next investigate how ML-deep trenches are formed during annealing by *in situ* LEEM observations. Figure 5 shows LEEM images of the Si-deposited epitaxial graphene obtained during annealing at 890−900 °C. The surface is mostly covered with BL, and ML and TL are, respectively, seen brighter and darker than BL. In the areas indicated by square *A*, the islands move slowly (at most 5 nm/s) while producing bright linear contrast, indicating that the ML-deep trenches are formed with the island motion. The way how the islands move is understood in more detail from the AFM and LEEM images in Figs. 3 and 4. The islands generally move in random directions. Although some of the islands move along the substrate steps as indicated by arrows in Fig. 3(a), the island motion is rather insensitive to the steps.

In Fig. 5, we can also find that the Si island jumps by a distance significantly longer than the atomic scale without trench formation as indicated by an arrow in rectangle *C* between Figs. 5(a) and 5(b). Such long jumps are initiated at lower temperatures than the trench formation. This phenomenon supports the weak interaction between the Si island and the epitaxial graphene, but we do not understand when and where the Si islands start forming the trenches. The defects in graphene are probably the trigger points.

Furthermore, Fig. 5 shows the other type of structural change in rectangles *B* and *C*. The bright contrast of ML graphene becomes dimmer at the same time when the islands at the boundary between ML and BL shrink in size. This suggests that Si atoms inside the islands are intercalated at the interface between the buffer layer and the SiC substrate. Reference [15] showed that the Si intercalation changes the epitaxial ML graphene into quasifreestanding BL graphene. Figures 6(a) and 6(b) show the LEEM images before and after Si intercalation. Some of the ML areas, indicated by white squares in (b), changed their image intensity levels during annealing. The bottom (purple) curves in Fig. 6(c) shows the

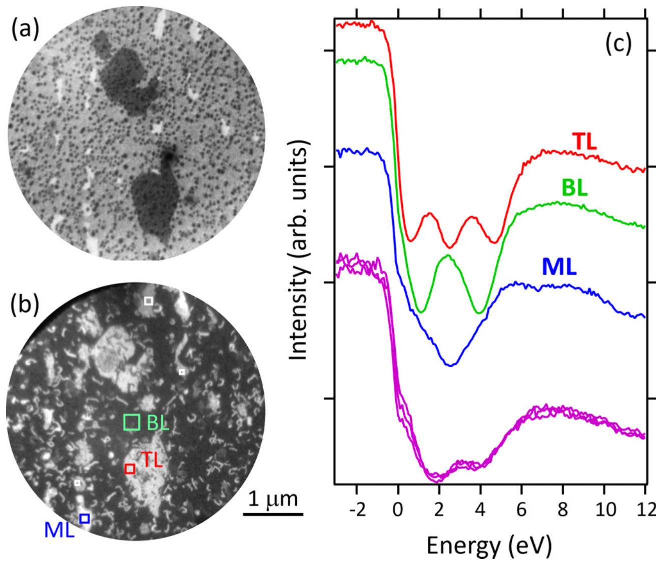

FIG. 6. LEEM images of Si-deposited epitaxial graphene (a) during annealing at 730 °C and (b) after annealing at 790 °C. The electron-beam energies were (a) 6.0 and (b) 4.0 eV. The ML areas look the brightest in (a). Some of the ML areas as exemplified by the areas indicated by white squares in (b) were intercalated by Si atoms. (c) LEER spectra from the areas indicated by squares in (b). Bottom purple curves correspond to the spectra from the white squares. The LEER spectra of ML, BL, and TL graphene were measured from the areas with corresponding colors. Spectra of each color are shifted vertically for clarity.

LEER spectra obtained from these intercalated areas. They provide two dips within the electron-beam energy of 0–6 eV as contrasted with epitaxial ML graphene having only one dip in this energy window of the LEER spectrum, which indicates the formation of quasifreestanding BL graphene [15].

Figure 7(a) shows a cross-sectional TEM image of the island after annealing at 970 °C. The FFT patterns from the island and the substrate are, respectively, shown in Figs. 7(b) and 7(c). These FFT patterns prove that the island has epitaxial relationship with the substrate and is lattice matched. The initial Si islands are transformed into the SiC islands during annealing. The Si islands incorporate carbon atoms from graphene, resulting in trenches on the surface. In other words, the Si island motion is driven by carbonization of Si. The island motion continues until the composition becomes SiC. All the AFM and LEEM results indicate that the trenches are ML deep, which is also supported by the TEM image in Fig. 7(d) showing a ML-deep trench between red triangles.

The carbon silicon phase diagram indicates that Si, SiC, and graphite are phase separated in a solid state [24]. However, it is known that bimetallic components, which are immiscible in bulk, can form homogeneous alloy nanoparticles [25]. Alloying of C and Si is likely to be allowed in nanometer-sized islands, and the weak interaction between the alloy island and the graphene should favor a smaller contact area, which probably limits the trench depth to ML. However, graphene sheets are not clearly imaged at the island/substrate interface in Fig. 7(a), suggesting that the SiC islands penetrate

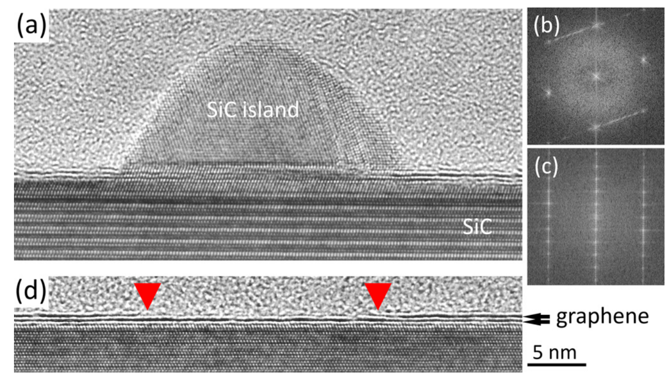

FIG. 7. (a) Cross-sectional TEM image of a SiC island after annealing at 970 °C. FFT patterns from (b) the island area, and (c) the substrate area in (a). (d) Cross-sectional TEM image of a ML-deep trench, which are indicated by two triangles.

all the graphene layers at the final stage of the carbonization reaction.

The ML-deep trenches are formed on epitaxial graphene thicker than or equal to BL, but not on ML graphene. The Si intercalation rather than the trench formation takes place in the ML area. The *in situ* LEEM observations also indicate that the BL areas adjacent to the buffer layer change their intensities even at lower temperatures around 550 °C, suggesting that Si atoms are intercalated easily through the buffer layer. The buffer layer seems to be a preferential diffusion path of Si atoms to the buffer layer/SiC interface. This is consistent with the reported results that Pb atoms penetrate through the buffer layer via defects during annealing, and that ML graphene is transformed to quasifreestanding BL graphene from the boundary with the buffer layer [26]. Si atoms are shown to be reactive enough to etch graphene at high temperatures. When ML graphene is etched by the carbonization reaction, the Si island should make contact with the buffer layer. The buffer layer is much more permeable to Si atoms than epitaxial graphene. Thus, the Si islands do not continue the trench formation in ML, but the Si atoms are intercalated into the interface.

In addition, the comparison between Figs. 4(a) and 4(c) indicates that the ML and BL areas, respectively, widened at the ML/BL and BL/TL boundaries after annealing at 1130 °C as exemplified by the ML area indicated by dotted lines. This suggests that the intercalated Si atoms are unstable against annealing at higher temperatures. They diffuse along the interface and react with the buffer layer to restore SiC. There are always edges of the buffer layer at the boundaries between the areas with different numbers of graphene layers. These edges should be preferential reaction sites with Si atoms, resulting in the expansion of thinner epitaxial graphene from such boundaries.

It is well known that mobile metal nanoparticles form trenches in graphene/graphite along specific crystallographic directions during annealing in a H_2 ambient [27,28]. This phenomenon is known as nanocutting. The trenches start from the edges/steps of graphene/graphite, and the depth is the same as the height of the steps. The metal nanoparticles serve as catalysts for hydrogenation of graphene lattices, and, therefore,

nanocutting can form trenches without limitation of length. On the other hand, the length of the trenches found in this paper should be determined by the number of Si atoms in the islands, which is supported by Fig. S1(c) in the Supplemental Material showing that the trench length increases with the volume of the islands after the motion [29]. Besides, they are not aligned along any crystallographic direction of graphene as confirmed by Fig. S2 in the Supplemental Material in which many trenches are gathered by setting their starting points to an origin [29]. We checked a possibility of Si island motion along the boundaries between the stacking domains in BL graphene [30] but find no correlation between the trenches and the stacking domain boundaries. The different roles of the islands in the reaction with graphene, direct carbonization and catalytic hydrogenation, might be the reason discriminating whether the trench formation is nondirectional or directional. It is known that the Au islands move on Si(111) with ML-deep trenches left behind [31]. This trench formation is caused by alloying of the Au islands with Si and is rather nondirectional. There might be some common mechanism regardless of the difference in the material system.

IV. SUMMARY

In this paper, we investigated structural changes in Si-deposited epitaxial graphene during annealing. Annealing causes Si islands to move with producing ML-deep trenches in the epitaxial graphene thicker than ML. These islands which terminated their motion are made of SiC. During annealing, Si islands are carbonized into SiC islands by incorporating carbon atoms from graphene, resulting in the etching of graphene. The carbonization reaction of Si is a driving force of the Si island motion. In the ML graphene area, the Si atoms released from the islands are intercalated at the buffer layer/SiC interface, probably via the etch pit formed in ML by the carbonization reaction. The reaction pathway of Si and epitaxial graphene is distinctly different depending on the number of graphene layers

ACKNOWLEDGMENTS

This work was partly supported by JSPS KAKENHI Grants No. 20H05670 and No. 21H01768.

[1] Y. M. Lin, C. Dimitrakopoulos, K. A. Jenkins, D. B. Farmer, H. Y. Chiu, A. Grill, and P. Avouris, Science **327**, 662 (2010).

[2] Y. M. Lin, A. Valdes-Garcia, S. J. Han, D. B. Farmer, I. Meric, Y. N. Sun, Y. Q. Wu, C. Dimitrakopoulos, A. Grill, P. Avouris, and K. A. Jenkins, Science **332**, 1294 (2011).

[3] K. V. Emtsev, A. Bostwick, K. Horn, J. Jobst, G. L. Kellogg, L. Ley, J. L. McChesney, T. Ohta, S. A. Reshanov, J. Rohrl, E. Rotenberg, A. K. Schmid, D. Waldmann, H. B. Weber, and T. Seyller, Nature Mater. **8**, 203 (2009).

[4] S. Tanaka, K. Morita, and H. Hibino, Phys. Rev. B **81**, 041406(R) (2010).

[5] J. S. Bunch, S. S. Verbridge, J. S. Alden, A. M. van der Zande, J. M. Parpia, H. G. Craighead, and P. L. McEuen, Nano Lett. **8**, 2458 (2008).

[6] S. Hu, M. Lozada-Hidalgo, F. C. Wang, A. Mishchenko, F. Schedin, R. R. Nair, E. W. Hill, D. W. Boukhvalov, M. I. Katsnelson, R. A. W. Dryfe, I. V. Grigorieva, H. A. Wu, and A. K. Geim, Nature (London) **516**, 227 (2014).

[7] M. Lozada-Hidalgo, S. Hu, O. Marshall, A. Mishchenko, A. N. Grigorenko, R. A. W. Dryfe, B. Radha, I. V. Grigorieva, and A. K. Geim, Science **351**, 68 (2016).

[8] P. Z. Sun, Q. Yang, W. J. Kuang, Y. V. Stebunov, W. Q. Xiong, J. Yu, R. R. Nair, M. I. Katsnelson, S. J. Yuan, I. V. Grigorieva, M. Lozada-Hidalgo, F. C. Wang, and A. K. Geim, Nature (London) **579**, 229 (2020).

[9] C. Riedl, C. Coletti, T. Iwasaki, A. A. Zakharov, and U. Starke, Phys. Rev. Lett. **103**, 246804 (2009).

[10] C. Virojanadara, A. A. Zakharov, S. Watcharinyanon, R. Yakimova, and L. I. Johansson, New J. Phys. **12**, 125015 (2010).

[11] S. Oida, F. R. McFeely, J. B. Hannon, R. M. Tromp, M. Copel, Z. Chen, Y. Sun, D. B. Farmer, and J. Yurkas, Phys. Rev. B **82**, 041411(R) (2010).

[12] I. Gierz, T. Suzuki, R. T. Weitz, D. S. Lee, B. Krauss, C. Riedl, U. Starke, H. Hochst, J. H. Smet, C. R. Ast, and K. Kern, Phys. Rev. B **81**, 235408 (2010).

[13] A. L. Walter, K. J. Jeon, A. Bostwick, F. Speck, M. Ostler, T. Seyller, L. Moreschini, Y. S. Kim, Y. J. Chang, K. Horn, and E. Rotenberg, Appl. Phys. Lett. **98**, 184102 (2011).

[14] K. V. Emtsev, A. A. Zakharov, C. Coletti, S. Forti, and U. Starke, Phys. Rev. B **84**, 125423 (2011).

[15] C. Xia, S. Watcharinyanon, A. A. Zakharov, R. Yakimova, L. Hultman, L. I. Johansson, and C. Virojanadara, Phys. Rev. B **85**, 045418 (2012).

[16] M. G. Silly, M. D'Angelo, A. Besson, Y. J. Dappe, S. Kubsky, G. Li, F. Nicolas, D. Pierucci, and M. Thomasset, Carbon **76**, 27 (2014).

[17] A. Visikovskiy, S.-i. Kimoto, T. Kajiwara, M. Yoshimura, T. Iimori, F. Komori, and S. Tanaka, Phys. Rev. B **94**, 245421 (2016).

[18] A. Markevich, R. Jones, S. Öberg, M. J. Rayson, J. P. Goss, and P. R. Briddon, Phys, Rev. B **86**, 045453 (2012).

[19] R. Sakakibara and W. Norimatsu, Phys. Rev. B **105**, 235442 (2022).

[20] H. Hibino, H. Kageshima, F. Maeda, M. Nagase, Y. Kobayashi, and H. Yamaguchi, Phys. Rev. B **77**, 075413 (2008).

[21] S. W. Poon, W. Chen, E. S. Tok, and A. T. S. Wee, Appl. Phys. Lett. **92**, 104102 (2008).

[22] Z. Ben Jabra, M. Abel, F. Fabbri, J. N. Aqua, M. Koudia, A. Michon, P. Castrucci, A. Ronda, H. Vach, M. De Crescenzi, and I. Berbezier, ACS Nano **16**, 5920 (2022).

[23] H. Hibino, H. Kageshima, and M. Nagase, J. Phys. D:Appl. Phys. **43**, 374005 (2010).

[24] T. B. Massalski, H. Okamoto, P. R. Subramanian, and L. Kacprzak (eds.), *Binary Alloy Phase Diagrams*, 2nd ed. (ASM International, Materials Park, OH, 1990), Vol. 3.

[25] J. Luo, M. M. Maye, V. Petkov, N. N. Kariuki, L. Wang, P. Njoki, D. Mott, Y. Lin, and C.-J. Zhong, Chem. Mater. **17**, 3086 (2005).

[26] D. Yang, Q. F. Xia, H. T. Gao, S. F. Dong, G. Y. Zhao, Y. F. Zeng, F. Ma, and T. W. Hu, Appl. Surf. Sci. **569**, 151012 (2021).

[27] S. S. Datta, D. R. Strachan, S. M. Khamis, and A. T. C. Johnson, Nano Lett. **8**, 1912 (2008).
[28] L. Ci, Z. Xu, L. Wang, W. Gao, F. Ding, K. F. Kelly, B. I. Yakobson, and P. M. Ajayan, Nano Res. **1**, 116 (2008).
[29] See Supplemental Material at https://link.aps.org/supplemental/10.1103/PhysRevMaterials.7.054003 for the relationship between the length of the trenches and the volume of the islands after the motion, and the trace of the motion of the islands.
[30] H. Hibino, S. Mizuno, H. Kageshima, M. Nagase, and H. Yamaguchi, Phys. Rev. B **80**, 085406 (2009).
[31] H. Hibino and Y. Watanabe, Surf. Sci. **588**, L233 (2005).